Reduced Order Modeling for Transonic Aeroservoelastic Control Law Development

Josiah M. Waite,* Bret K. Stanford,† Walter A. Silva,† and Robert E. Bartels‡
NASA Langley Research Center, Hampton, VA, 23681

As aircraft become more flexible, aeroelastic considerations become increasingly important and complex, particularly for transonic flight where nonlinearities in the flow render linear analysis tools less effective. In order to analyze these aeroelastic interactions between the fluid and the structure efficiently, reduced order models (ROMs) are sometimes generated from and used in place of computational fluid dynamics solutions. In this paper, several aerodynamic ROMs are generated and coupled with structural models to form aeroelastic ROMs. The aerodynamic ROMs generated here include the effects of control surface motion. Hence, the aeroelastic ROMs presented here are appropriate for use in aeroservoelastic applications and are intended to be used for aeroservoelastic control law development. These ROMs are used to simulate a number of test cases with and without control surface involvement. Results show that several of the ROMs generated in the paper are able to predict results similar to solutions of higher-order computational methods.

Nomenclature

ASE	=	Aeroservoelastic
CFD	=	Computational fluid dynamics
CRM	=	Common research model
DLM	=	Doublet lattice method
GAF	=	Generalized aerodynamic force
ROM	=	Reduced order model
$\boldsymbol{A}$	=	Structural state matrix
b	=	Wingspan
$\boldsymbol{b}$	=	Damping matrix
$\boldsymbol{B}$	=	Structural input matrix
$\boldsymbol{C}$	=	Structural output matrix
$\boldsymbol{f}$	=	Structural input vector
$\boldsymbol{k}$	=	Stiffness matrix
$\boldsymbol{m}$	=	Mass matrix
q	=	Dynamic pressure
$\boldsymbol{x}$	=	Structural state vector
y	=	Wing spanwise coordinates
$\boldsymbol{y}$	=	Structural output vector
$\boldsymbol{\eta}$	=	Generalized displacement vector
$\boldsymbol{\omega}$	=	Natural frequency vector
ζ	=	Damping ratio

*Research Aerospace Engineer, Aeroelasticity Branch, MS 340, AIAA Member, josiah.m.waite@nasa.gov
†Research Aerospace Engineer, Aeroelasticity Branch, MS 340, AIAA Associate Fellow
‡Research Aerospace Engineer, Aeroelasticity Branch, MS 340, AIAA Senior Member

I. Introduction

As aircraft designs tend toward wings with higher aspect ratio and increasing flexibility, interactions between structural dynamics and aerodynamics become more complex. These complex interactions have historically been analyzed within a framework that includes computational models for the structure and fluid. Typically, a linear formulation (such as a doublet lattice method, or DLM) has been used for the fluid solver to keep the computational cost of the analysis down[1–5]. With more complex aircraft designs, however, the ability to generate accurate, nonlinear aerodynamic predictions becomes increasingly essential [6]. This is especially true for aircraft with cruise speeds in the transonic regime as linear tools are often not equipped to account for nonlinearities in the transonic flow. Although researchers have successfully integrated higher-order CFD solvers into computational aeroelastic models (Refs. 7–11), it is still considered to be a challenge because of the high computational cost [12], particularly for unsteady simulations.

Reduced order modeling is an alternative to directly implementing CFD solvers into aeroelastic analysis frameworks [13]. These reduced order models (ROMs) are typically (but not always [14–16]) linearized systems derived from CFD data and so contain information regarding the nonlinear behavior of the fluid, which makes them particularly well-suited as analysis tools for transonic flows [14, 16–19]. If the ROM has been properly formulated, parameters within the ROM can be changed and results for new configurations or conditions can be generated in much less time than would be required by another CFD simulation [15, 20].

Previously, the authors compared results from ROMs generated with two different techniques to results from a DLM code and results from an unsteady Reynolds-averaged Navier-Stokes simulation [17]. The results suggested that the ROMs were capturing information about the nonlinearities in the flow that were not captured by the DLM that allowed the ROM to perform better in aeroservoelastic (ASE) applications. This work is a continuation of that work. Here, several more aeroelastic ROMs are generated for use in ASE applications. The paper will first present some of the compuational tools used to generate the ROMs, then the differences between the various ROM-generation techniques will be discussed. Finally, results from the several ROMs will be compared.

II. Methods

A. Geometry

The analyses presented here were conducted on a semispan model of the NASA Common Research Model (CRM; see Fig. 1) as developed in Ref. 21. This is a generic transport geometry with a cruise Mach number of 0.85, wing span of 58.7 meters, mean aerodynamic chord of 7 meters, aspect ratio of 9, taper ratio of 0.275, and sweep angle of 35°. Results presented in this paper are at a Mach number of 0.85 and angle of attack of 0°. Two trailing edge control surfaces were attached to the wing as shown in the bottom of Fig. 1. When deflected, the edges of each trailing edge control surface were blended into the trailing edge of the wing, as shown in the top right of Fig. 1.

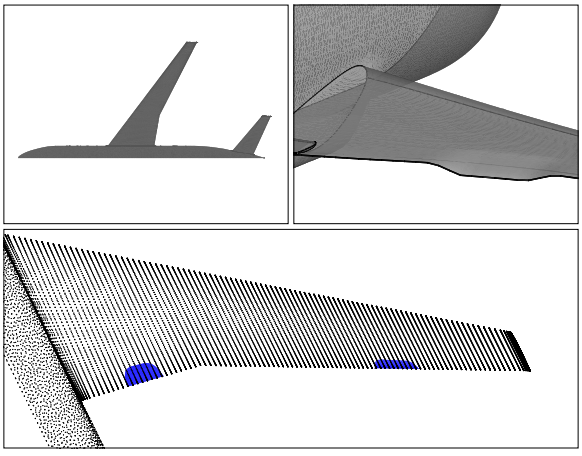

Fig. 1 Top left: Visualization of the NASA CRM semispan model used in the current analysis. Top right: Illustration of one control surface deflection. Note the control surface blending. Bottom: Representation of the two control surfaces used in the current model, with control surface #1 near the root and control surface #2 near the tip.

Only the wing was considered to be flexible in this work, populated with an aluminum wingbox built from ribs, spars, skins, and stiffeners, described more fully in Ref. 21. The wingbox was connected to a series of lumped masses meant to emulate fuel and engine inertia. A total of 25 flexible structural modes and two rigid control modes (where the control surfaces were assumed to be irreversible, or rigid with rigid hinges) were generated for this geometry. The two control modes represented a unit rotation in the control surface while holding the rest of the wing fixed. The control surfaces associated with the two control modes were located at $2y/b = 0.214$ and 0.787. Modes 1, 2, 3, and 8 were the most influential modes in the vehicle's overall motion, so they are the modes for which visualizations are presented here. Figure 2 shows (qualitatively) the vertical deflection magnitudes for modes 1, 2, 3, and 8, which had natural frequencies of 10.7, 23.6, 26.4, and 85.0 rad/s, respectively.

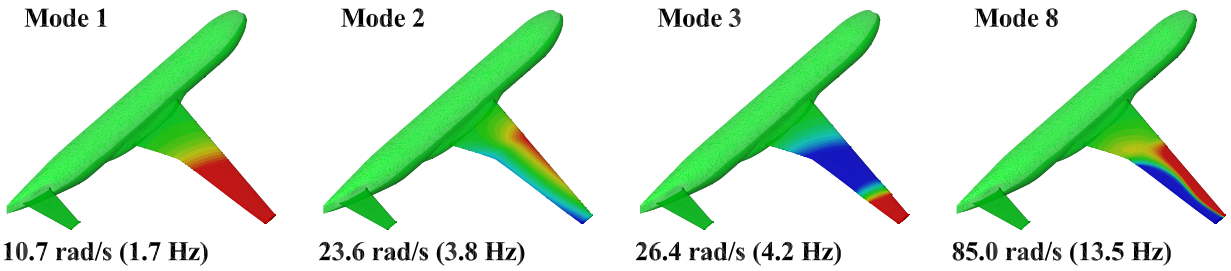

Fig. 2 Vertical deflections and frequencies associated with modes 1, 2, 3, and 8.

B. FUN3D

The NASA Langley Research Center FUN3D code was used to conduct all CFD simulations for this work. FUN3D is primarily a computational fluid dynamics solver, but it also has a built-in modal structural dynamics solver that uses a second-order accurate predictor-corrector scheme.

For all CFD results used here (which include training simulations and test case simulations), a converged steady flow solution with a rigid aircraft configuration was obtained. A static aeroelastic simulation was then restarted from the converged steady solution. The converged static aeroelastic solution was the starting point for each of the ROMs presented in this paper; however, the training simulation for each ROM proceeded differently. In some cases, once the static aeroelastic simulation reached a converged state, a dynamic aeroelastic simulation was restarted from the static solution. In this dynamic simulation, control modes were excited and the modal structural dynamics equations were solved at each iteration along with the fluid dynamics equations. In the dynamic simulations for other cases, a combination of control and structural modes were excited and the modal structural dynamics equations were not solved.

For all FUN3D analyses, the unsteady Reynolds-averaged Navier-Stokes equations were solved using a second-order upwind scheme with a Spalart-Allmaras turbulence model. A fairly coarse semi-infinite tetrahedral volume mesh was used here, with 3.1 million nodes, and a y+ value nearly 1 throughout the surface.

No validation or verification data will be presented here for this computational mesh beyond a mesh convergence study shown in Ref. 22 because this work has less to do with generating accurate CFD results and more to do with generating ROMs that capture what is predicted by CFD. Hence, the FUN3D solution will be used as the "truth" model here without extensive testing for how accurate its solutions actually are. Naturally, the better the training solution is at capturing real physics, the better the ROM will be.

C. AEROM

AEROM [18] is a set of tools particularly suited to generating aeroelastic ROMs. Before generating the ROM itself, a training simulation was completed, which, in this case, was performed using FUN3D. Modal data was passed to FUN3D, including mode shapes and modal frequencies, for use in the analysis. In the simulation, a number of modes of interest were excited simultaneously, generally by disturbing modal displacements. Different excitation profiles can be used, including Gaussian pulses or sines and cosines. In the cases presented here, orthogonal Walsh functions [23] were used. The length of the Walsh inputs and the step size used were tailored to capture a desired frequency range. Note that these two parameters, along with the number of modes being excited simultaneously, will often have to be balanced against available resources as they affect the duration of the simulation. Determining the magnitudes of the Walsh

functions was less straightforward than determining their lengths, as this quantity is often configuration-dependent. In the cases presented here, the magnitudes of excitations to the structural modes were based on converged static aeroelastic deflections, while magnitudes of excitations to control modes were kept between 1° and 3°.

After determining the shape of the excitation profiles and running the training simulation, a set of modal responses (in the form of generalized aerodyamic forces, GAFs) due to the modal excitations was generated. These modal responses become input to an algorithm within AEROM that extracted individual impulse responses of desired modes to the inputs and converted them to a state-space system using an eigensystem realization algorithm. In this way, a state-space reduced-order model was generated from a higher-order training simulation.

AEROM has a built-in subroutine that creates a state-space model of the modal structural dynamics of a vehicle. This structural model is generally integrated into a loop with the aerodynamic ROM to produce a unified, aeroelastic ROM. Inputs to the structural model include generalized masses, modal frequencies, and modal damping. For the cases presented in this paper, these parameters came from NASTRAN.

Using AEROM, FUN3D, and the geometry described previously, three classes of aeroelastic ROMs were generated for this work. These three classes of ROMs are referred to in this text as ROM-I, ROM-II, and ROM-III.

D. ROM-I

Before discussing ROM-I in detail, it is important to note that the modes for which FUN3D produces modal responses are not limited to the set of modes that were excited. For example, consider a training simulation where the modal structural dynamics equations are solved alongside the fluid dynamics (as is possible in FUN3D). If six modes were included in the training simulation, but only two of them were excited, and if the four unexcited modes were allowed to evolve in response to those excitations, then modal responses for the four unexcited modes could be generated. This would lead to a ROM where the fluid-structure interactions at a given dynamic pressure would be captured at the level of the training simulation. Such was the case with ROM-I. In contrast, consider a training simulation where no structural dynamics equations are solved and, therefore, there is no modeling of the interactions between fluid and structure in the training simulation. In order to generate modal responses for the four previously unexcited modes, they would need to be excited along with the previously excited two modes. The ROM produced from this training simulation would represent only aerodynamic effects, usually in the form of generalized aerodynamic forces, of each excited mode on all other excited modes. In other words, the ROM produced from this training simulation would be an aerodynamic ROM, not an aeroelastic ROM. In order to generate an aeroelastic ROM, the structural dynamics equations would need to be solved by a separate, uncoupled structural dynamics model that would pass structural information to the aerodynamic ROM. In this formulation of the aeroelastic ROM, the fluid-structure interactions would be handled at the level of the lower-order aerodynamic and structural models instead of at the level of the higher-order training simulation. ROM-II (see Fig. 6) and ROM-III (see Fig. 8) are examples of this type of formulation. This important distinction will be helpful in the following discussions of ROM-I, ROM-II, and ROM-III.

ROM-I was essentially identical to ROM-W from Ref. 17. The excitation profiles for the two control modes that were excited in the training simulation for ROM-I are shown in Fig. 3. No structural modes were excited here. The training simulation produced output data for all 25 structural modes, but only the first 10 were used to generate ROM-I. Because this training simulation included a step to solve the structural dynamics, ROM-I was only valid for the dynamic pressure used in the training simulation, which was 17kPa. Furthermore, the resultant ROM was inherently aeroelastic as it had the aeroelastic interactions embedded within it. In other words, no additional models had to be added to the ROM generated from this training simulation to allow it to simulate aeroelastic phenomena. This fact is illustrated by its

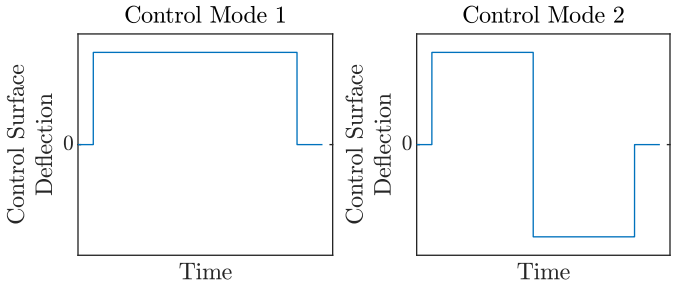

Fig. 3 Excitation profiles for the two control modes that were excited in the training simulation for ROM-I.

simple block diagram, shown in Fig. 4. Note that the inputs for ROM-I were two control mode displacements and the outputs were the first 10 structural mode displacements.

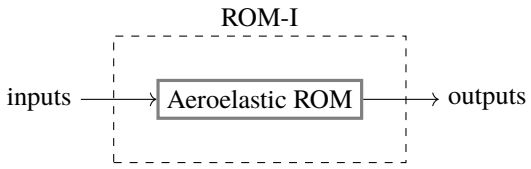

Fig. 4 Block diagram of ROM-I. Because the ROM that was generated from AEROM already had aeroelastic effects embedded inside it, no additional structural model was needed to allow ROM-I to handle aeroelastic analyses. However, this model was only valid for a single dynamic pressure. Inputs for ROM-I were two control mode displacements and outputs were modal displacements of 10 modes of interest.

E. ROM-II

ROM-II is the second ROM examined here and improved on ROM-I. In order to generate a ROM that was valid over a range of dynamic pressures, the training simulation for ROM-II did not solve the structural dynamics equations. Instead of generating an aeroelastic ROM directly from the training simulation, the training simulation was used to generate an aerodynamic ROM whose outputs were aerodynamic forces (GAFs) imposed on the structural modes. In order to output accurate GAFs for each structural mode of interest, impulse responses of each structural mode due to the motion of every other structural mode of interest was generated in addition to the impulse responses of the structural modes due to the motion of the control modes. To accomplish this in the training simulation, each structural mode of interest was excited along with the control modes. To keep computational cost reasonable, it was necessary to use less modes than the 10 used in ROM-I. It was determined (using a separate code to solve modal structural dynamics and doublet-lattice aerodynamics) that structural modes 1, 2, 3, and 8 contributed the most to the vehicle's overall motion, so these modes were used to generate ROM-II. The general excitation profiles of these four structural modes and the two control modes are shown in Fig. 5.

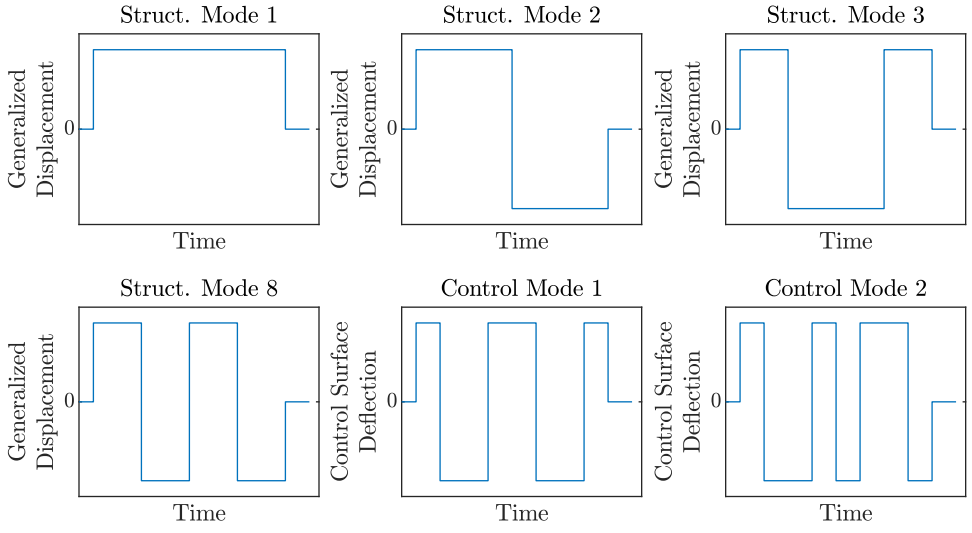

Fig. 5 Excitation profiles for the four structural modes and two control modes used in the training simulation for ROM-II.

In order to make ROM-II capable of aeroelastic analyses, a structural model was coupled with the aerodynamic ROM generated from the training simulation, as shown in Fig. 6. The aerodynamic ROM had six inputs (six generalized displacements – two for the control modes, which are external inputs, and four for the structural modes of interest from the structural model) and four outputs (GAFs for each of the structural modes of interest – GAFs applied the control modes were inconsequential as the control surfaces were modeled as perfectly rigid and irreversible). The states of

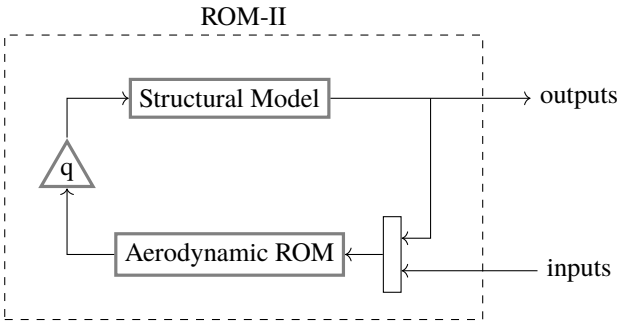

Fig. 6 Block diagram for ROM-II. Because the training simulation did not include steps to solve the structural dynamics equations, a structural model was needed to enable ROM-II to handle aeroelastic analyses. This allowed ROM-II to vary dynamic pressure, q. Inputs for ROM-II were two control mode displacements and outputs were modal displacements of four modes of interest.

the aerodynamic ROM were aerodynamic states internal to the ROM generation process – no physical meaning has been associated with any of these states at this time. Likewise, the state, input, output, and feedthrough matrices of the aerodynamic state-space ROM were only meaningful internally to the aerodynamic ROM and were governed by the algorithms inside AEROM. The structural model implemented in ROM-II was a state-space model of the structural equations of motion. Here, the structural model had four inputs (GAFs for each of the structural modes of interest, scaled by some dynamic pressure) and four outputs (generalized displacements for each of the structural modes of interest). Hence the aeroelastic ROM-II had two control surface inputs and four outputs, which were the generalized displacement for each of the stuctural modes of interest. The general equations of motion used in the development of the structural model can be written as

$$\boldsymbol{m}\ddot{\boldsymbol{\eta}} + \boldsymbol{b}\dot{\boldsymbol{\eta}} + \boldsymbol{k}\boldsymbol{\eta} = \boldsymbol{f} \tag{1}$$

where, in this case, $\boldsymbol{m}$ was a 4×4 mass matrix, $\boldsymbol{b}$ was a 4×4 damping matrix, and $\boldsymbol{k}$ was a 4×4 stiffness matrix. The 4×1 state vector, $\boldsymbol{\eta}$, contained the generalized displacements of the four structural modes of interest. The 4×1 input vector, $\boldsymbol{f}$, contained the GAFs for each of the structural modes of interest. Again, note that GAFs applied to each control surface were not needed here since the control surfaces were modeled as perfectly rigid and irreversible. The stiffness and damping matrices can be rewritten in terms of the mass matrix, natural frequencies, ω, and damping ratio, ζ:

$$\begin{aligned} \boldsymbol{k} &= \boldsymbol{\omega}^2\boldsymbol{m} \\ \boldsymbol{b} &= 2\zeta\boldsymbol{\omega}\boldsymbol{m} \end{aligned}$$

where $\boldsymbol{\omega}$ is a 4×4 matrix with natural frequency values on the diagonal. Making these substitutions into Eq. 1 and rearranging yielded:

$$\ddot{\boldsymbol{\eta}} + 2\zeta\boldsymbol{\omega}\dot{\boldsymbol{\eta}} + \boldsymbol{\omega}^2\boldsymbol{\eta} = \boldsymbol{m}^{-1}\boldsymbol{f} \tag{2}$$

Eq. 2 was converted into a state-space model with four inputs, four outputs, and eight states of the form:

$$\begin{aligned} \dot{\boldsymbol{x}} &= \boldsymbol{A}\boldsymbol{x} + \boldsymbol{B}\boldsymbol{f} \\ \boldsymbol{y} &= \boldsymbol{C}\boldsymbol{x} \end{aligned} \tag{3}$$

where components of Eq. 3 were defined as follows:

$$\boldsymbol{A} = \begin{bmatrix} 0 & 0 & 0 & 0 & 1 & 0 & 0 & 0 \\ 0 & 0 & 0 & 0 & 0 & 1 & 0 & 0 \\ 0 & 0 & 0 & 0 & 0 & 0 & 1 & 0 \\ 0 & 0 & 0 & 0 & 0 & 0 & 0 & 1 \\ -\omega_{1,1}^2 & 0 & 0 & 0 & -2\zeta\omega_{1,1} & 0 & 0 & 0 \\ 0 & -\omega_{2,2}^2 & 0 & 0 & 0 & -2\zeta\omega_{2,2} & 0 & 0 \\ 0 & 0 & -\omega_{3,3}^2 & 0 & 0 & 0 & -2\zeta\omega_{3,3} & 0 \\ 0 & 0 & 0 & -\omega_{4,4}^2 & 0 & 0 & 0 & -2\zeta\omega_{4,4} \end{bmatrix}$$

$$\boldsymbol{B} = \begin{bmatrix} 0 & 0 & 0 & 0 \\ 0 & 0 & 0 & 0 \\ 0 & 0 & 0 & 0 \\ 0 & 0 & 0 & 0 \\ 1/m_{1,1} & 0 & 0 & 0 \\ 0 & 1/m_{2,2} & 0 & 0 \\ 0 & 0 & 1/m_{3,3} & 0 \\ 0 & 0 & 0 & 1/m_{4,4} \end{bmatrix}$$

$$\boldsymbol{C} = \begin{bmatrix} 0 & 0 & 0 & 0 & 1 & 0 & 0 & 0 \\ 0 & 0 & 0 & 0 & 0 & 1 & 0 & 0 \\ 0 & 0 & 0 & 0 & 0 & 0 & 1 & 0 \\ 0 & 0 & 0 & 0 & 0 & 0 & 0 & 1 \end{bmatrix}$$

$$\boldsymbol{x} = \begin{bmatrix} \eta_1 \\ \eta_2 \\ \eta_3 \\ \eta_4 \\ \dot{\eta}_1 \\ \dot{\eta}_2 \\ \dot{\eta}_3 \\ \dot{\eta}_4 \end{bmatrix}$$

In order to assess the sensitivity of the ROM to changes in the conditions of the training simulation, two parameters within the training simulation were varied: (1) the dynamic pressure at which training simulation was executed (2) and the amplitude of the modal excitations. These variations resulted in four training simulation conditions, presented here as:

- "a" - This was the baseline condition, run at a dynamic pressure of 16,942 Pa. The training simulation had Walsh input amplitudes of 2° for the control surfaces and 5% of the static aeroelastic point for each of the flexible modes (for example, if the static displacement for mode 1 was 100, then the Walsh amplitude applied mode 1 for the training simulation was 5).
- "b" - This training simulation was run at an identical dynamic pressure as "a", but the ratio of control mode excitation amplitude to structural mode excitation amplitude was increased.
- "c" - This training simulation was run at a higher dynamic pressure relative to "a", but with the same ratio of control mode excitation amplitude to structural mode excitation amplitude as "a".
- "d" - This training simluation was run at both higher dynamic pressure and higher ratio of control mode excitation amplitude to structural mode excitation amplitude relative to "a".

These variations are denoted in the results by appending identifiers to each ROM (for example, ROM-IIa represents the ROM-II model whose training simulation conditions correspond to "a" above, and so on).

As shown in Fig. 7a, the dynamics of ROM-II were highly sensitive to the conditions at which the training simulation occurred. It was postulated that the resulting differences in the reduced-order system dynamics may have been a result of exciting the structural modes and control modes simultaneously in the training simulations. A third and final ROM configuration, ROM-III, was developed to explore that possibility.

F. ROM-III

Instead of having a single aerodynamic ROM that was generated from a single training simulation that excited control and structural modes together simultaneously (as was the case for ROM-II), ROM-III included two aerodynamic ROMs that came from two separate training simulations, one each for control mode excitations and structural mode excitations.

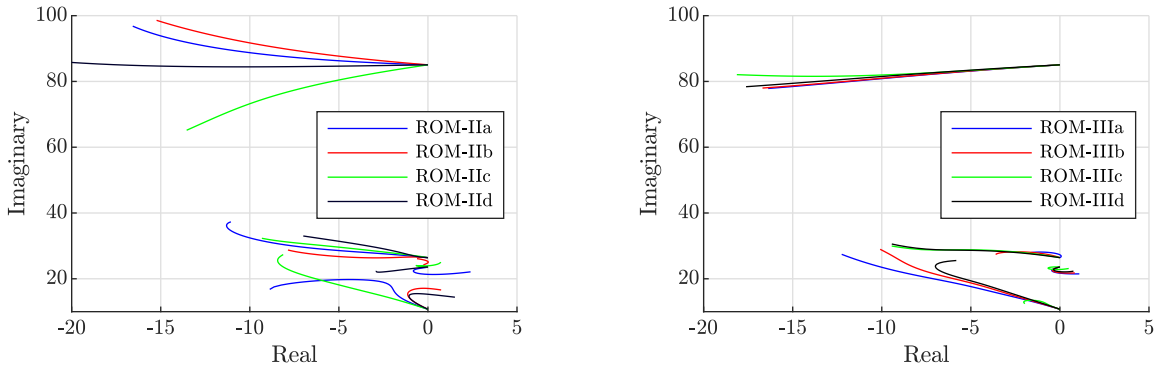

Fig. 7 Root locus plot for (a) ROM-II and (b) ROM-III across several training simulation conditions. Note that these plots do not involve control surface motion.

To generate the aerodynamic ROM for the structural modes, its corresponding training simulation excited four structural modes only. The same four structural modes (1, 2, 3, and 8) and structural mode excitation profiles were used here as in the aerodynamic ROM of ROM-II (see Fig. 5). No control mode excitations occurred in this particular training simulation.

To generate the aerodynamic ROM for the control modes, its corresponding training simulation excited the two control modes only. The same two control mode excitation profiles were used here as in the aeroelastic ROM of ROM-I (see Fig. 3). No structural mode excitations occurred in this particular training simulation.

The structural model for ROM-III was identical to that of ROM-II. The combination of the aerodynamic ROMs and structural model for ROM-III is shown in Fig. 8. The training simulations used to generate ROM-III were varied in the same ways as those for ROM-II. A comparison of the resulting root locus plots for those variations is shown in Fig. 7b. Compared to the root locus plots for the same variations in ROM-II (Fig. 7a), there was a significant improvement in the similarity of system dynamics across different training conditions.

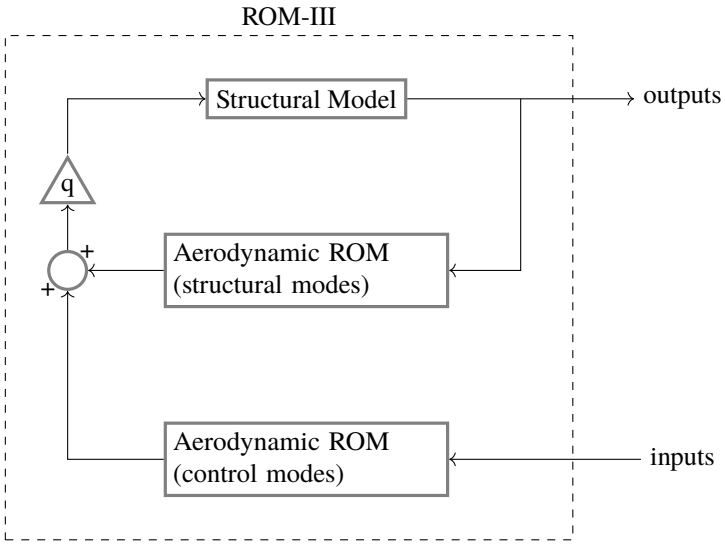

Fig. 8 Block diagram for ROM-III. Two aerodynamic ROMs were produced and used in ROM-III: one strictly for structural modes and the other strictly for control modes. This was done to decouple any unwanted interactions between the control and structural modes in the training simulations. Like ROM-II, ROM-III needed an additional structural model that would allow for aeroelastic analyses at different dynamic pressures. Inputs for ROM-III were two control mode displacements and outputs were modal displacements of four modes of interest.

III. Results

Figure 9, which is simply a magnified version of Fig. 7, labels the dynamic pressures at which the real parts of these unstable modes change sign, indicating a change in stability. Previously, a full-order model was used to bracket the flutter point for this geometry, and it was found to be about 30.3 kPa[22]. Ignoring the modes in Fig. 9 that go unstable but then return to stability (which may or may not be physical), each flutter point as predicted by the ROMs is between 31.3 and 39.1 kPa, which compares well with FUN3D's prediction. Additionally, ROM-II is not consistent about which mode number goes unstable, whereas ROM-III consistently predicts mode 2 to go unstable (again, ignoring the modes that go unstable then return to stability).

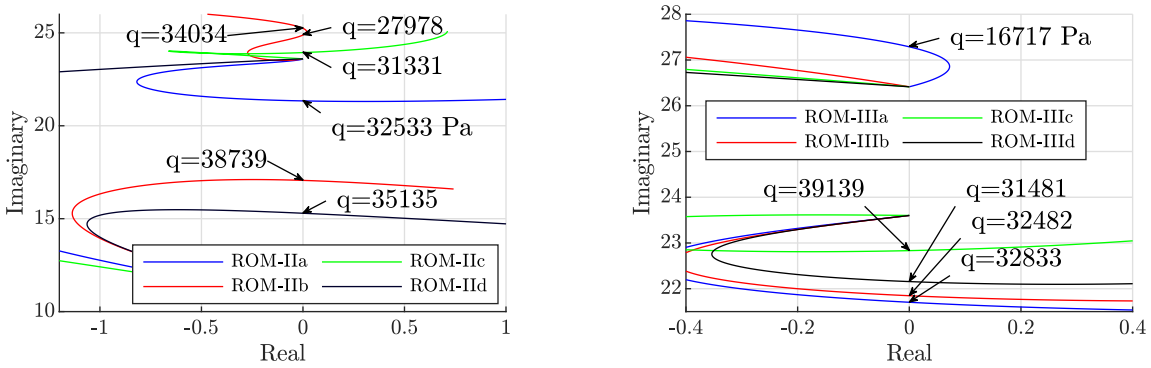

Fig. 9 Root locus plot for (a) ROM-II and (b) ROM-III across several training simulation conditions, magnified to see modal instabilities. Dynamic pressures at which the real part of each unstable mode changes sign are marked.

To further explore the quality of each of the ROMs discussed so far, several were exercised in two test cases. In order for a ROM to be effective in ASE applications, it must be able to capture the free response (i.e., the response of each structural mode due to the motion of every other structural mode) as well as the forced response due to control surface motion (i.e., the response of each structural mode due to the motion of control surfaces). Hence, the two test cases presented here highlight each ROM's ability to perform these two tasks. Portions of the results are shown and discussed here.

For the first test case, a disturbance was introduced to the system and the structural modes were allowed to respond. In this case, control surface displacement inputs were zero, meaning the simulation was simply the free response due to whatever initial conditions were present in the states. The initial condition for the first modal velocity was given a nonzero value while all other initial conditions were fixed to zero. FUN3D, ROM-II, and ROM-III were all used to model this case, and results were obtained for several dynamic pressures (3.1, 9.5, 16.9, 25.7, and 35.0 kPa). Note that ROM-I was not exercised for this test case because access to the structural mode states was not as straightforward as with the other models. Recall that, because the training simulation for ROM-I solved the structural dynamics equations internally, the structural states were embedded within whatever states came out of the AEROM algorithms. The information needed to describe the behavior of the structural modes was contained in the states of ROM-I, but knowing which states correlated to specific structural modes was not clear. No attempt was made, therefore, to model this case using ROM-I.

For brevity, results for only three dynamic pressures (3.1, 16.9, and 35.0 kPa) from each solver are shown in Figs. 10, 11, and 12. For clarity, the whole solution is not shown; rather, a magnified view of the last time steps is shown to illustrate the difference between the codes. A careful comparison of all the results reveals that, for all five dynamic pressures examined, ROM-IIId performed the best, matching the FUN3D results more closely than the other ROM-II and ROM-III models.

For the second test case, the structural modes were allowed to respond to control mode inputs. In this case, sinusoidal inputs of varying frequencies were applied to the modal displacement of control surface #2 at a dynamic pressure of 16.9 kPa. The open-loop responses were computed by each ROM and compared to those from FUN3D. Figure 13 shows the frequency response functions of each ROM compared to FUN3D. Immediately apparent are frequencies at which some models appear to give unrealistically high amplitudes, as is the case for ROM-IId near frequency values of 14 rad/s and ROM-IIb near frequency values of 25 rad/s and ROM-IIIa near frequency values of 27 rad/s. Recall that the natural frequencies of modes 1, 2, and 3 are 10.7, 23.6, and 26.4 rad/s, respectively, and so these inaccuracies in the

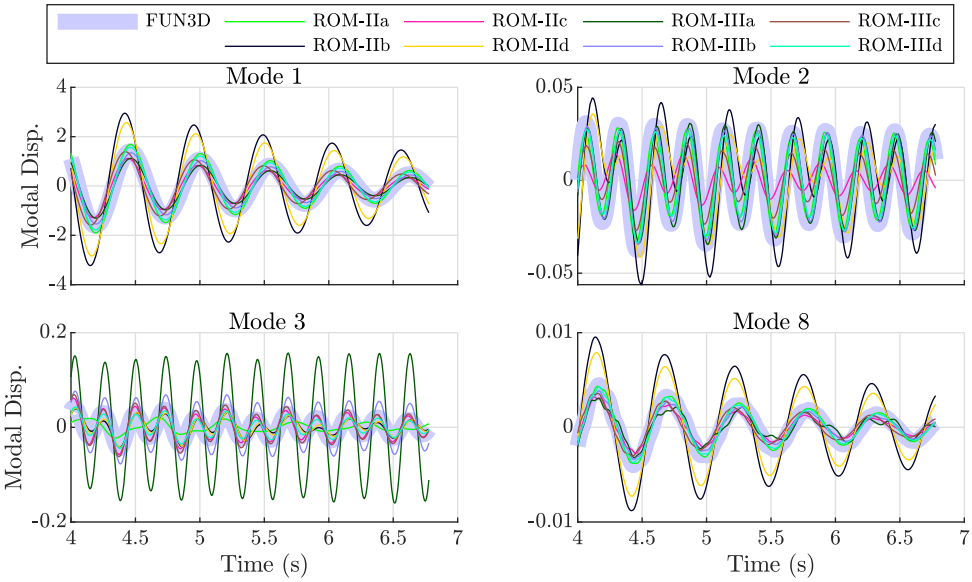

Fig. 10 Free response due to a nonzero initial condition in first modal velocity at a dynamic pressure of 3.1 kPa.

results may be due to their proximity to natural frequencies. These predicted high amplitudes may cause nonlinear aerodynamic effects that are beyond the valid range of the linearized ROM, making the results difficult to interpret. Interestingly, ROM-I appears to do better than many of the ROM-II and ROM-III results. This is likely due to the fact that it was trained at the same dynamic pressure at which these test cases were run.

Time histories for a few frequencies (5, 12, 21, and 30 rad/s) are shown in Figs. 14-17. Again, while there is not one single ROM that is best for any one of these frequencies, there are some ROMs that consistently appear to be one that should *not* be used, such as ROM-IIb, ROM-IId, or ROM-IIIa (which, consequently, are the same ROMs idenitified above as being inaccurate based on results in Fig. 13). From these results, it seems that no one ROM generation technique will give accurate predictions over all conditions of interest, but several of them are close.

IV. Conclusion

Several methods for generating aeroelastic reduced order models were discussed here. The first method produced a ROM that captured aeroelastic effects well, but it was valid over a small range of dynamic pressures. The second method produced a ROM that was valid over a much wider range of dynamic pressures, but a number of uncertainties arose from the fact that its training simulation excited structural and control modes simultaneously. The third and final method produced a single aeroelastic ROM from two training simulations that was able to separate the effects of the control modes from the effects of the structural modes.

While there was no single ROM that seemed to outperform all the others in the test cases, it is significant that ROM-III, specifically ROM-IIId, fared best when only structural modes were involved. When choosing a method for generating an aeroelastic ROM, it appears that running separate training simulations for structural and control modes allows one to better capture what happens when only structural modes participate in a dynamic aeroelastic event. When control modes are involved, it appears that there is no significant advantage in executing separate training simulations, apart from the fact that one might be able to have shorter runtimes for each training simulation.

The aeroelastic ROMs presented in this paper will be used to generate controllers and observers that will be implemented into a closed-loop feedback loop within FUN3D. Active flutter suppression will then be demonstrated.

Acknowledgments

This work is funded by the NASA Advanced Air Transport Technologies project. The authors would like to acknowledge the support of Dr. Steven Massey for his help in generating computational meshes used in this work.

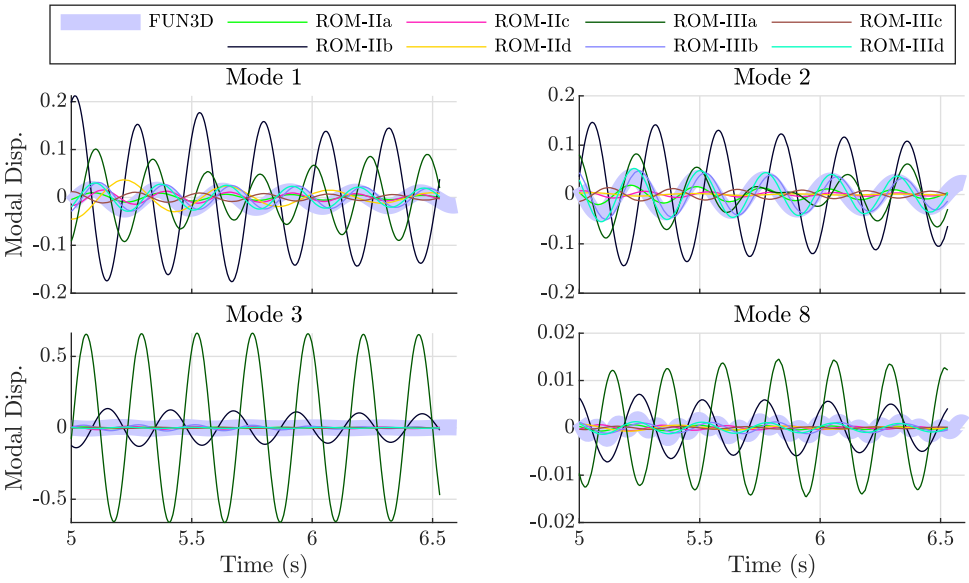

Fig. 11 Free response due to a nonzero initial condition in first modal velocity at a dynamic pressure of 16.9 kPa.

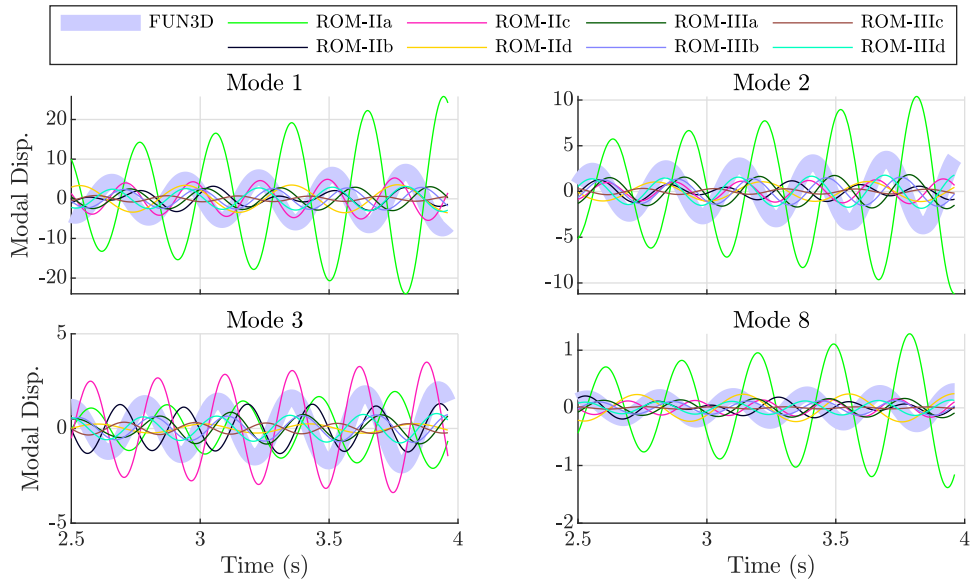

Fig. 12 Free response due to a nonzero initial condition in first modal velocity at a dynamic pressure of 35.0 kPa.

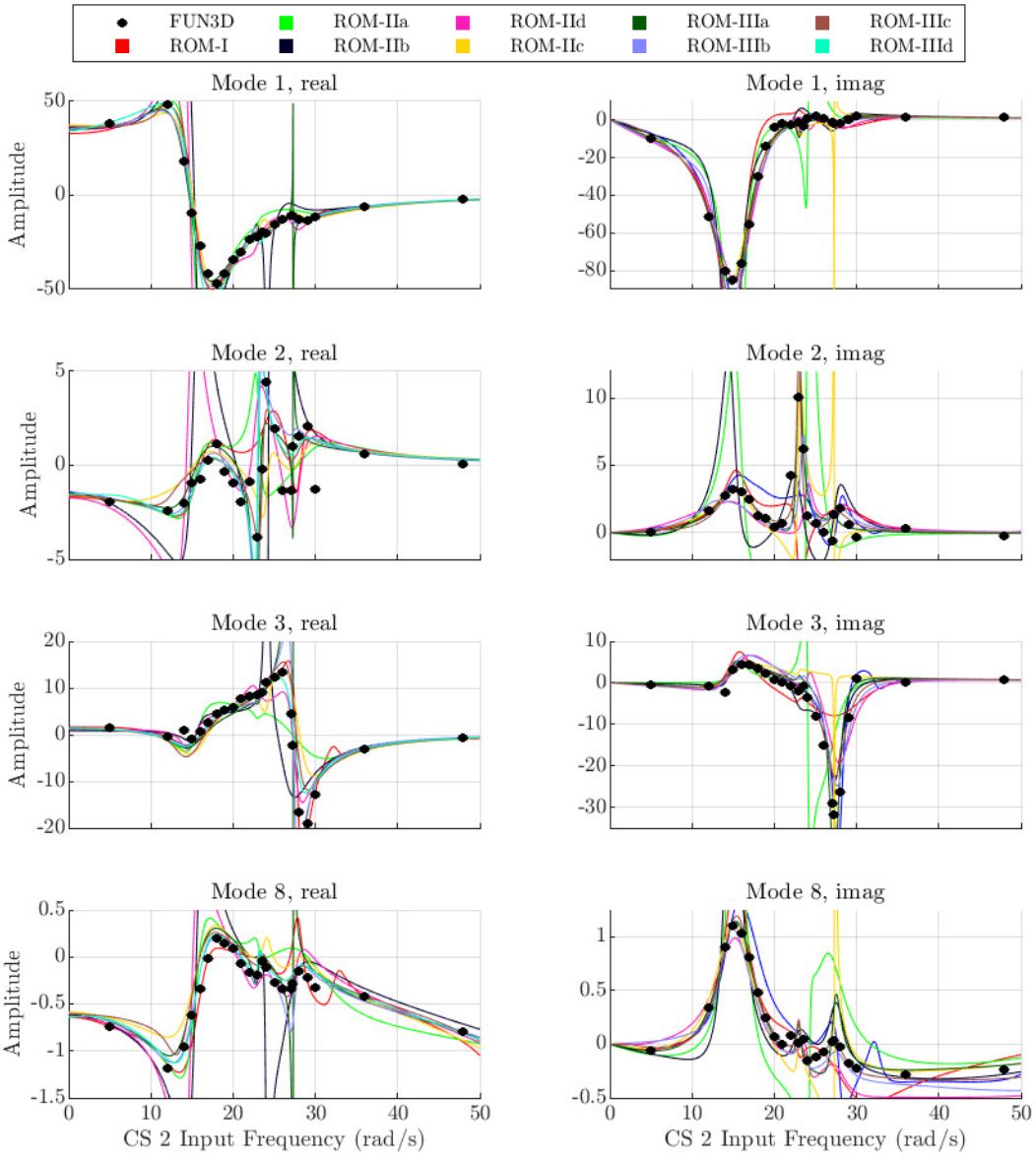

Fig. 13 Frequency response functions for control surface #2 inputs.

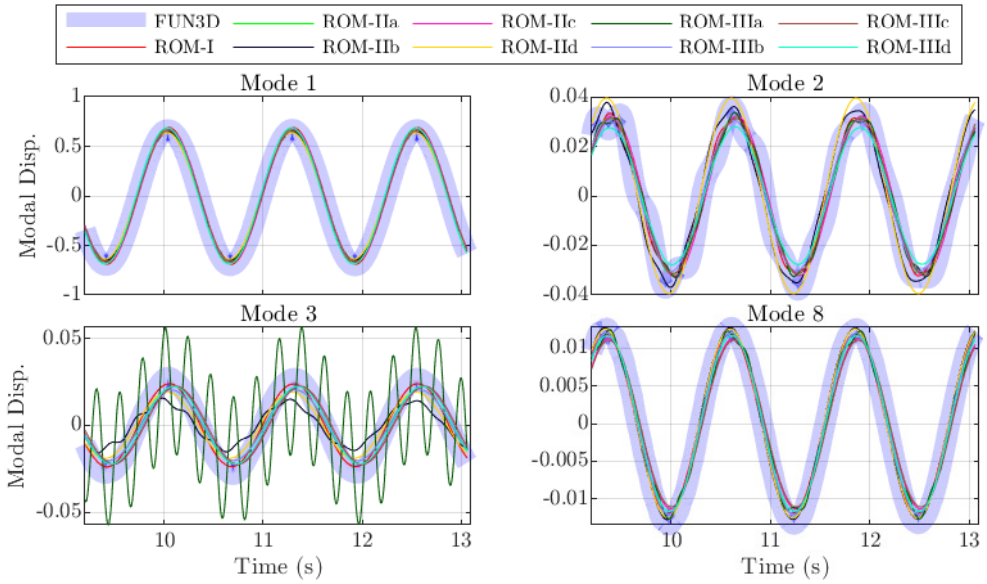

Fig. 14 Time history of the modal response to a sinusoidal input signal applied to control surface #2 at 5 rad/s.

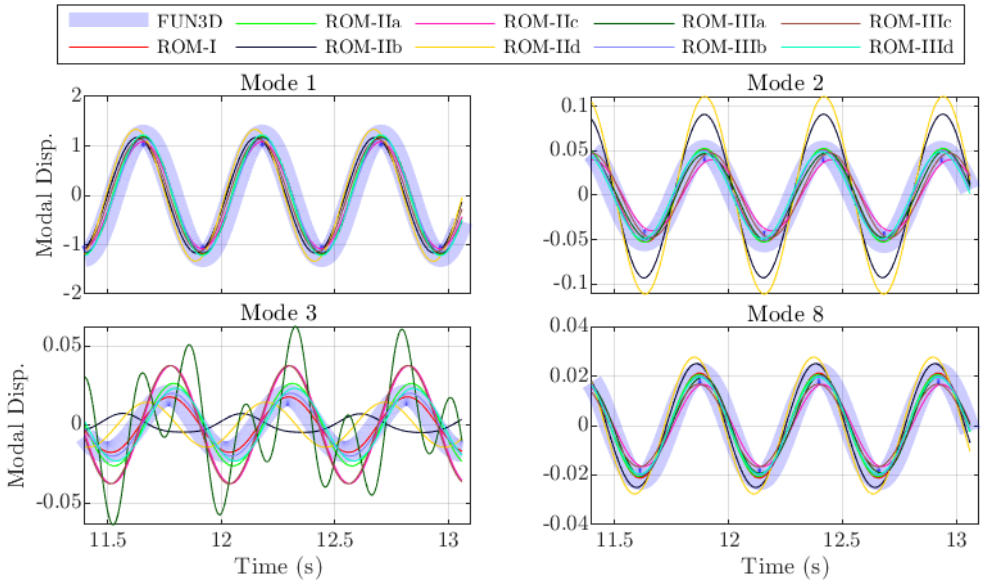

Fig. 15 Time history of the modal response to a sinusoidal input signal applied to control surface #2 at 12 rad/s.

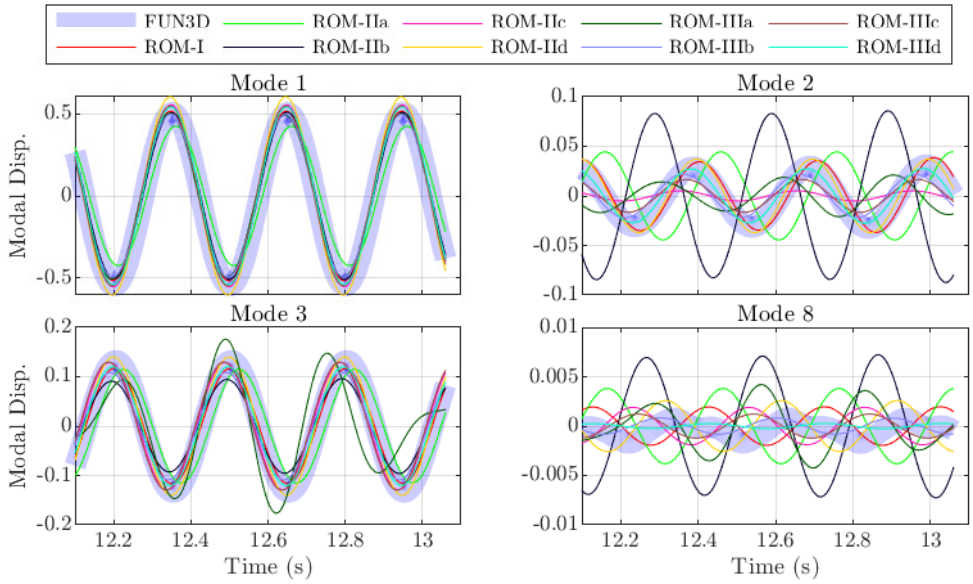

Fig. 16 Time history of the modal response to a sinusoidal input signal applied to control surface #2 at 21 rad/s.

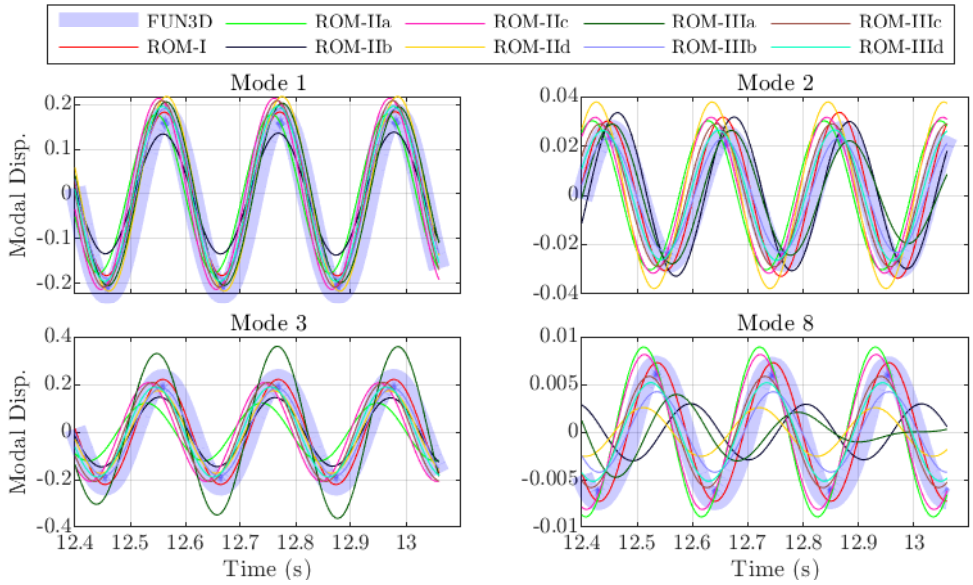

Fig. 17 Time history of the modal response to a sinusoidal input signal applied to control surface #2 at 30 rad/s.

References

[1] Qian, W., Huang, R., Hu, H., and Yonghui, Z., "Active Flutter Suppression of a Multiple-Actuated-Wing Wind Tunnel Model," *Chinese Journal of Aeronautics*, Vol. 27, No. 6, 2014, pp. 1451–1460.

[2] Burnett, E., Beranek, J., Holm-Hansen, B., Atkinson, C., and Flick, P., "Design And Flight Test of Active Flutter Suppression on the X-56A Multi-Utility Technology Test-Bed Aircraft," *The Aeronautical Journal*, Vol. 120, No. 1228, 2016, pp. 893–909.

[3] Ting, E., Chaparro, D., and Nguyen, N. T., "Development of an Integrated Nonlinear Aeroservoelastic Flight Dynamic Model of the Truss-Braced Wing Aircraft," *58th AIAA/ASCE/AHS/ASC Structures, Structural Dynamics, and Materials Conference*, Grapevine, TX, 9-13 Jan 2017.

[4] Wang, Y., Wynn, A., and Palacios, R., "Nonlinear Modal Aeroservoelastic Analysis Framework for Flexible Aircraft," *AIAA Journal*, 2016, pp. 3075–3090.

[5] Zhao, Y., "Flutter Suppression of a High Aspect-Ratio Wing with Multiple Control Surfaces," *Journal of Sound and Vibration*, Vol. 324, No. 3-5, 2009, pp. 490–513.

[6] Afonso, F., Vale, J., Oliveira, É., Lau, F., and Suleman, A., "A Review on Non-Linear Aeroelasticity of High Aspect-Ratio Wings," *Progress in Aerospace Sciences*, Vol. 89, 2017, pp. 40–57.

[7] Hallissy, B., and Cesnik, C., "High-Fidelity Aeroelastic Analysis of Very Flexible Aircraft," *52nd AIAA/ASME/ASCE/AHS/ASC Structures, Structural Dynamics and Materials Conference 19th AIAA/ASME/AHS Adaptive Structures Conference 13t*, Denver, CO, 4-7 Apr 2011.

[8] Brooks, T. R., Kenway, G. K., and Martins, J., "Undeflected Common Research Model (uCRM): An Aerostructural Model for the Study of High Aspect Ratio Transport Aircraft Wings," *35th AIAA Applied Aerodynamics Conference*, Denver, CO, 5-9 Jun 2017.

[9] Danowsky, B. P., Thompson, P. M., Farhat, C., Lieu, T., Harris, C., and Lechniak, J., "Incorporation of Feedback Control into a High-Fidelity Aeroservoelastic Fighter Aircraft Model," *Journal of Aircraft*, Vol. 47, No. 4, 2010, pp. 1274–1282.

[10] Danowsky, B. P., Lieu, T., and Coderre-Chabot, A., "Control Oriented Aeroservoelastic Modeling of a Small Flexible Aircraft using Computational Fluid Dynamics and Computational Structural Dynamics-Invited," *AIAA Atmospheric Flight Mechanics Conference*, San Diego, CA, 4-8 Jan 2016.

[11] Selitrennik, E., Karpel, M., and Levy, Y., "Computational Aeroelastic Simulation of Rapidly Morphing Air Vehicles," *Journal of Aircraft*, Vol. 49, No. 6, 2012, pp. 1675–1686.

[12] Tantaroudas, N. D., and Da Ronch, A., "Nonlinear Reduced-order Aeroservoelastic Analysis of Very Flexible Aircraft," *Advanced UAV Aerodynamics, Flight Stability and Control: Novel Concepts, Theory and Applications*, 2017, p. 143.

[13] Lucia, D. J., Beran, P. S., and Silva, W. A., "Reduced-Order Modeling: New Approaches for Computational Physics," *Progress in Aerospace Sciences*, Vol. 40, No. 1-2, 2004, pp. 51–117.

[14] Zhang, W., Wang, B., Ye, Z., and Quan, J., "Efficient Method for Limit Cycle Flutter Analysis Based on Nonlinear Aerodynamic Reduced-Order Models," *AIAA journal*, Vol. 50, No. 5, 2012, pp. 1019–1028.

[15] Kou, J., and Zhang, W., "Reduced-Order Modeling for Nonlinear Aeroelasticity with Varying Mach Numbers," *Journal of Aerospace Engineering*, Vol. 31, No. 6, 2018, p. 04018105.

[16] Zhang, W., Kou, J., and Wang, Z., "Nonlinear Aerodynamic Reduced-Order Model for Limit-Cycle Oscillation and Flutter," *AIAA Journal*, 2016, pp. 3304–3311.

[17] Waite, J., Stanford, B., Bartels, R. E., Silva, W. A., and Massey, S. J., "Active Flutter Suppression Controllers Derived from Linear and Nonlinear Aerodynamics: Application to a Transport Aircraft Model," *2018 Applied Aerodynamics Conference*, Atlanta, GA, 25-29 Jun 2018.

[18] Silva, W. A., "AEROM: NASA's Unsteady Aerodynamic and Aeroelastic Reduced-Order Modeling Software," *Aerospace*, Vol. 5, No. 2, 2018.

[19] Silva, W. A., and Bartels, R. E., "Development of Reduced-Order Models for Aeroelastic Analysis and Flutter Prediction Using The CFL3Dv6.0 Code," *Journal of Fluids and Structures*, Vol. 19, No. 6, 2004, pp. 729–745.

[20] Lieu, T., Farhat, C., and Lesoinne, M., "Reduced-Order Fluid/Structure Modeling of a Complete Aircraft Configuration," *Computer Methods in Applied Mechanics and Engineering*, Vol. 195, No. 41-43, 2006, pp. 5730–5742.

[21] Kenway, G., Kennedy, G., and Martins, J., "Aerostructural Optimization of the Common Research Model Configuration," *15th AIAA/ISSMO Multidisciplinary Analysis and Optimization Conference*, Altanta, GA, 16-20 Jun 2014.

[22] Stanford, B., and Massey, S. J., "Uncertainty Quantification of the FUN3D-Predicted Flutter Boundary on the NASA CRM," *58th AIAA/ASCE/AHS/ASC Structures, Structural Dynamics, and Materials Conference*, Grapevine, TX, 9-13 Jan 2017.

[23] Pacheco, R., and Steffen Jr, V., "Using Orthogonal Functions for Identification and Sensitivity Analysis of Mechanical Systems," *Modal Analysis*, Vol. 8, No. 7, 2002, pp. 993–1021.